Hindawi
Journal of Nanomaterials
Volume 2022, Article ID 1758789, 12 pages
https://doi.org/10.1155/2022/1758789

Research Article

Effects of Nitrogen-Doping or Alumina Films on Graphene as Anode Materials of Lithium-Ion Batteries Verified by In Situ XRD

Guang-Jhong Chen,[1] K. Y. Simon Ng,[2] and Chuen-Chang Lin[1]

[1]*Department of Chemical & Materials Engineering, National Yunlin University of Science and Technology, 123 University Road Sec. 3, Douliu, Yunlin 64002, Taiwan*
[2]*Department of Chemical Engineering and Materials Science, Wayne State University, Detroit, Michigan 48202, USA*

Correspondence should be addressed to Chuen-Chang Lin; linchuen@yuntech.edu.tw

Received 28 May 2022; Accepted 25 July 2022; Published 5 August 2022

Academic Editor: Senthil Kumaran Selvaraj

First, graphene is directly grown on nickel foil without additional catalysts by chemical vapor deposition (CVD). Next, the graphene is modified by nitrogen-doping, and alumina is deposited onto the graphene by magnetron sputtering. The charge-specific capacity of N-doped graphene is higher than that of graphene since 2 Theta of in situ XRD characteristic peaks for N-doped graphene moves toward a lower angle (about 24) which is smaller than that (about 25) for graphene, and then the gap between graphene layers for N-doped graphene is larger than that for graphene according to Bragg's Law, and N-doped graphene demonstrates the additional in situ XRD characteristic peak (LiC_6) in comparison to graphene only with the in situ XRD characteristic peak (LiC_{12}). Furthermore, because 2 Theta of in situ XRD characteristic peaks for Al_2O_3/graphene also moves toward a lower angle (about 24) and Al_2O_3/graphene also shows the additional in situ XRD characteristic peak (LiC_6), the charge-specific capacity of Al_2O_3/graphene is also higher than that of graphene.

1. Introduction

Lithium-ion batteries were applied to electric vehicles, portable electronic devices, etc. Compared with other batteries (such as Ni-Cd, lead-acid, and Ni-MH), lithium-ion batteries possess higher energy densities (100-150 $Wh\,kg^{-1}$), higher voltage, and lower maintenance [1, 2]. The performance of lithium-ion batteries mainly depends on the properties of anode and cathode materials [2]. In this research, we focused on anode materials of lithium-ion batteries.

In our previous study [3], carbon nanotubes, carbon nanotubes/graphene composites, and graphene were grown on nickel foil without additional catalysts by one-step ambient pressure CVD at 700°C, 800°C, and 900°C, respectively. The plateaus in the discharge/charge curves for graphene were more obvious than those for carbon nanotubes and carbon nanotubes/graphene composites during lithiation/delithiation processes; therefore, graphene was chosen to study lithiation/delithiation processes by in situ XRD. Furthermore, in our previous research [2, 3], the carbon nanotubes/graphene composite was doped by nitrogen, and alumina was deposited onto the N-doped carbon nanotubes/graphene composite, so graphene was modified by nitrogen-doping, and alumina was deposited onto graphene. Finally, in situ XRD was utilized to verify improvement of specific capacity for graphene after nitrogen-doping or being covered with alumina.

Dahn [4] observed scattering angles (2 Theta) in situ XRD characteristic peaks for crystalline synthetic graphite powder (KS-44) decreased with decreasing of predischarge

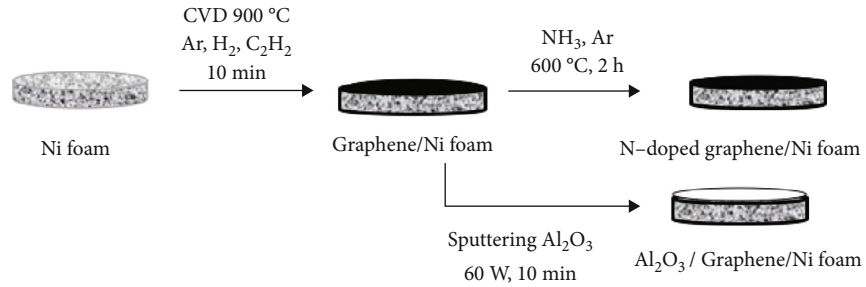

Figure 1: Schematic illustration of the fabrication process of graphene, N-doped graphene, and Al_2O_3/graphene.

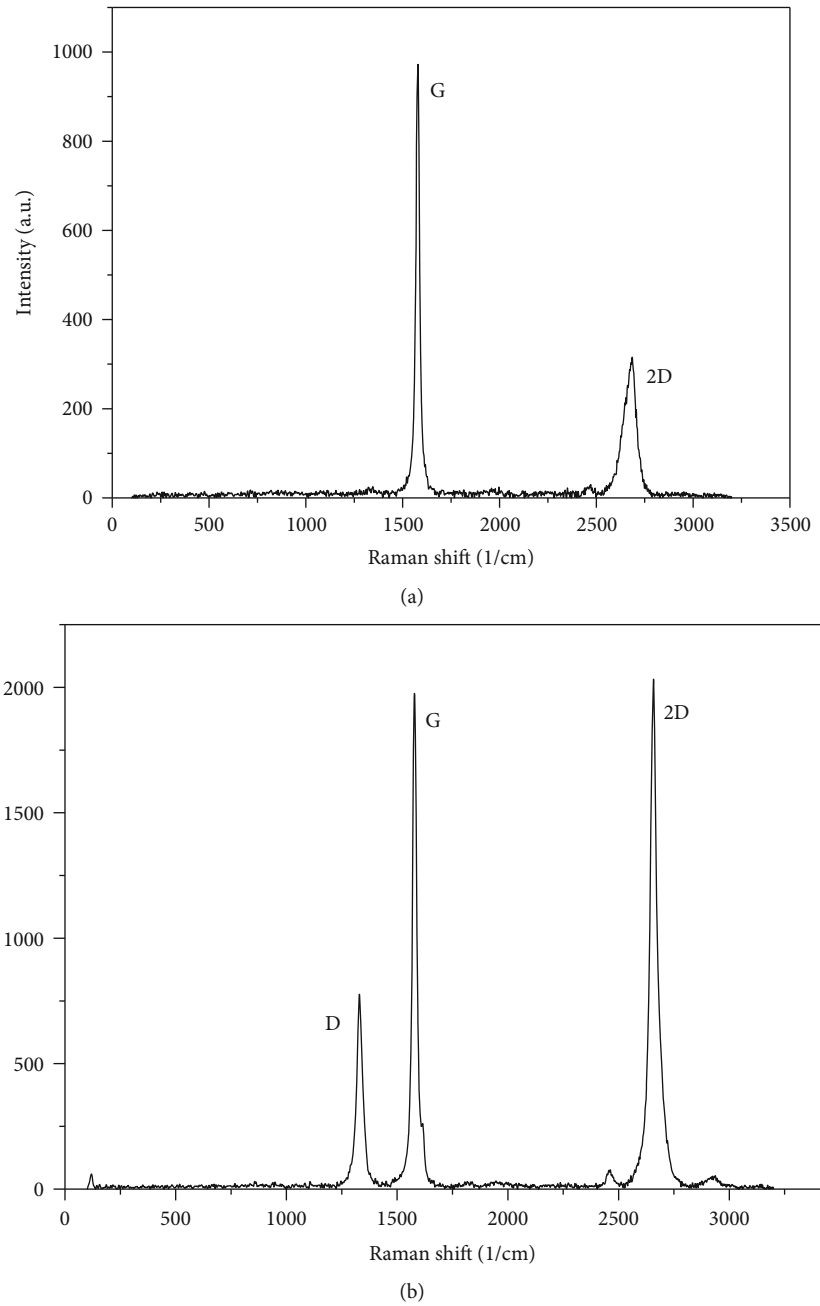

Figure 2: Raman spectra of (a) graphene and (b) N-doped graphene.

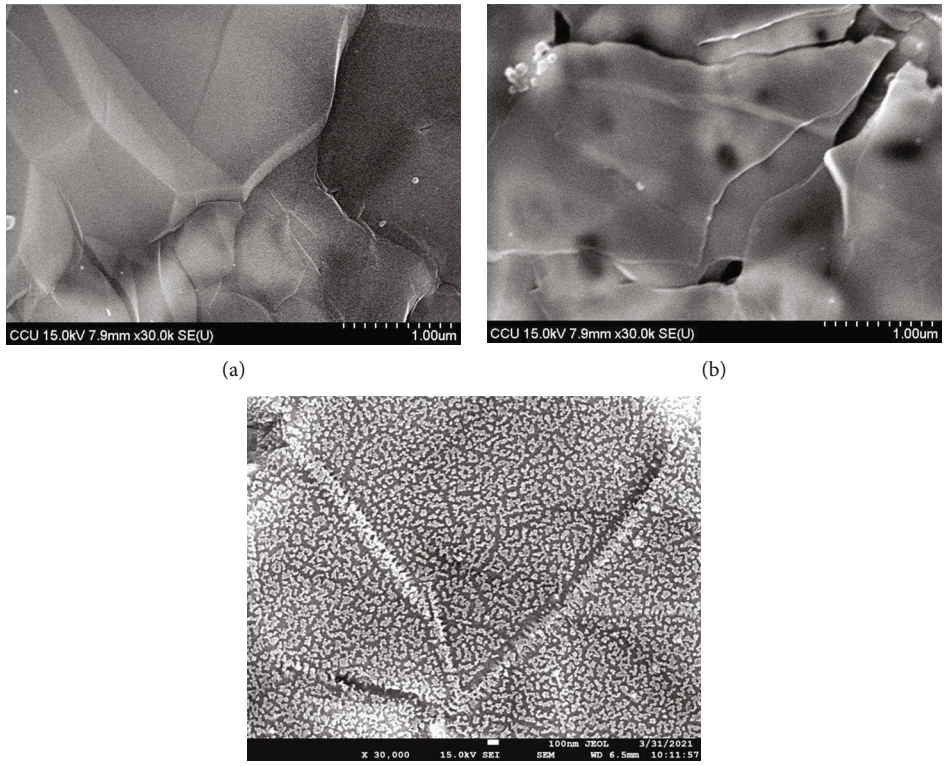

(a) (b)

(c)

Figure 3: The FESEM images of (a) graphene, (b) N-doped graphene, and (c) Al_2O_3/graphene.

voltages, so gaps between graphite layers (d) increased with decreasing of predischarge voltages due to d being inversely proportional to 2 Theta of in situ XRD characteristic peaks according to Bragg's Law. Furthermore, there are past studies that discuss nitrogen-doping. Wu et al. [5] mentioned that (1) to compensate for the poor performance of porous carbons, heteroatoms doping is considered to be an effective route to regulate corresponding electronic states and facilitate electron transfer, in which heteroatoms doping (such as N) is a common method to tailor the electronic conductivity of porous carbons; (2) the introduction of heteroatoms with different electronegativities from carbon can induce the charge density redistribution of carbon materials and lead to low band gap energy and rapid electron transfer on graphene basal planes; (3) heteroatoms possessing relatively large atomic sizes can further distort carbon structures and enlarge interlayer spacing to break balanced spin density and expose more electroactive defects (please see the revised manuscript). N-doped graphene possessed higher discharge capacity than graphene since N-doping induced defects and enlarged lattice spacing between graphene layers [6]. Pyridine-like local structures showed higher Li storage capacity because dangling bonds were formed by the rearrangement of C and N atoms around the divacancy sites that could stabilize intercalated Li atoms [7]. Moreover, literatures for alumina films were discussed. $Li_{1.2}Ni_{0.2}Mn_{0.2}Ru_{0.4}O_2$ (LNMR) with alumina coating as cathode materials for Li-ion batteries could enhance discharge capacity compared with uncoated LNMR [8]. $LiNi_{0.4}Mn_{0.4}Co_{0.2}O_2$ with alumina coating as cathodes showed increase of d-spacing with charging, with a slight delay in the onset of the increase state compared to the bare [9]. Multiwalled carbon nanotubes (MWCNTs) were grown on the Cu current collector by CVD, then alumina was deposited on the MWCNTs by atomic layer deposition, and alumina films could improve lithium-ion intercalation capacity [2, 10].

The main aim of this research was to verify improvement of specific capacity for graphene after nitrogen-doping or being covered with alumina; gap changes between graphene layers and difference of characteristic peaks (LiC_6 and LiC_{12}) for graphene with/without doping nitrogen and graphene being covered with/without alumina were analyzed by in situ XRD during lithiation/delithiation processes.

2. Materials and Methods

We followed the methods of Lin and Chang [3] to grow graphene on nickel foil without additional catalysts through one-step ambient pressure chemical vapor deposition (CVD) at 900°C. Next, graphene was N-doped with a gas mixture of NH3 (60 sccm) and Ar (250 sccm) for 2 h at 600°C [11]. Finally, alumina was deposited onto graphene

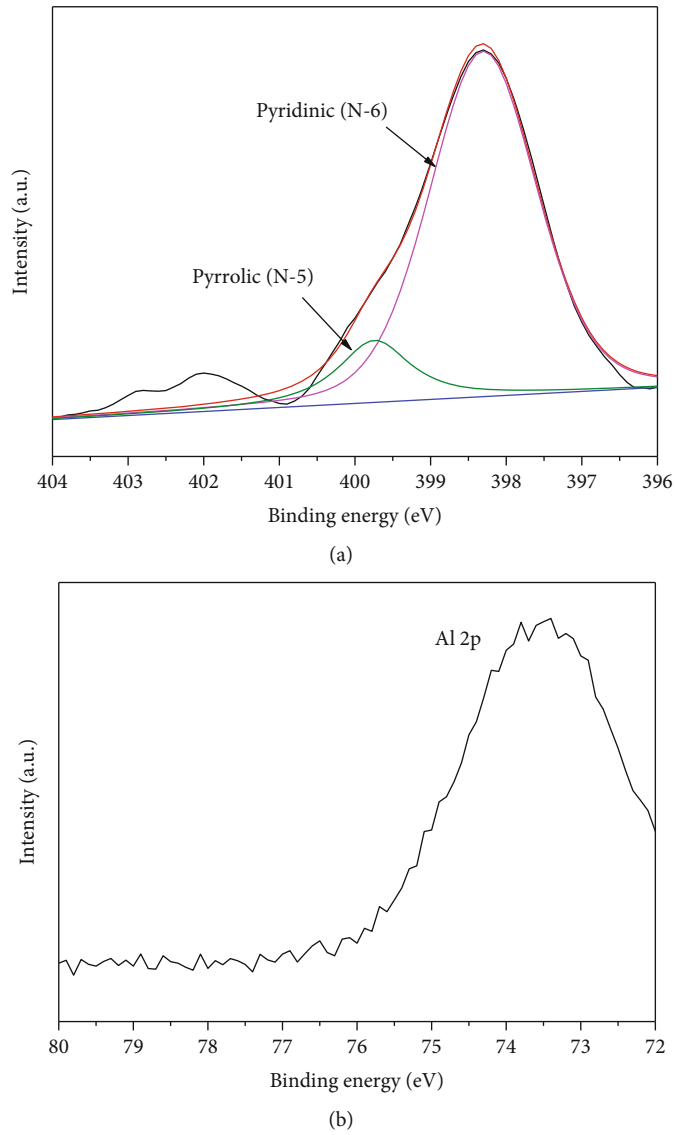

Figure 4: XPS spectra of (a) N-5 as well as N-6 for N-doped graphene and (b) Al 2P for Al_2O_3/graphene.

by RF magnetron sputtering at 60 W for 10 min according to our previous research [2].

A solution of 1 M $LiPF_6$ dissolved in 1: 1: 1 (wt%) ethylene carbonate-ethyl methyl carbonate-dimethyl carbonate from Ubiq Technology was used as the electrolyte [2]. The anode electrode ($\pi \times 0.65 \times 0.65\,cm^2$, Li metal: 99.9%, 0.3 mm thick, Ubiq Technology) was assembled with the cathode electrode ($\pi \times 0.65 \times 0.65$ cm^2, graphene or N-doped graphene or Al_2O_3/graphene) into a coin cell with the 0.1-0.15 ml electrolyte (1 M $LiPF_6$) and the PP/PE/PP separator (Celgard 2325, Celgard, USA) at room temperatures (about 293-303 K) by using a coin cell manual crimping machine (CR2032, Taiwan) in an Ar-filled glove box [2]. Furthermore, the assembly method of an in situ XRD coin cell is similar to that of the coin cell except for one additional piece of Be glass.

The D peak, G peak, and 2D peak for graphene and N-doped graphene were investigated by a microscopic Raman spectrometer (633 nm of wavelength; in Via, Renishaw, England). Furthermore, the Pyrrolic-N (N-5) and Pyridinic-N (N-6) XPS spectra of N-doped graphene and the Al 2p XPS spectrum of Al_2O_3 for the Al_2O_3/graphene were explored by XPS (Fison VG. ESCA210, England). Moreover, the structure of graphene, N-doped graphene, and Al_2O_3/graphene was conducted by field emission scanning electron microscope (FE-SEM) (JEOL JSM-6700F, Japan). Finally, cyclic voltammetry (CV) tests for graphene, N-doped graphene, and Al_2O_3/graphene were performed using an electrochemical analyzer (CH Instruments CHI 608B, USA) with the CR2032 coin cell over a potential range of 0.01-3.0 V at a scan rate of $0.1 mVs^{-1}$. Chronopotentiometry (CP) tests for graphene, N-doped graphene, and Al_2O_3/graphene were performed

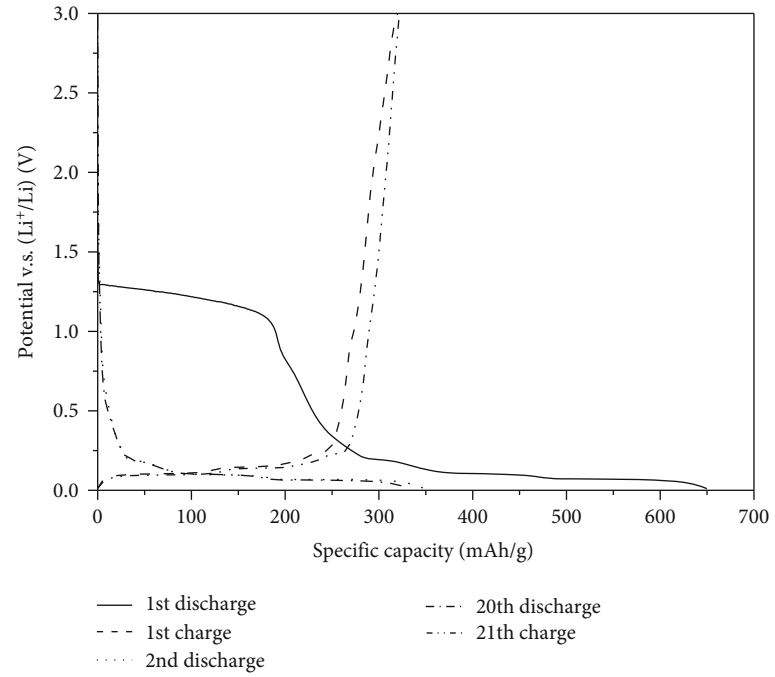

(a)

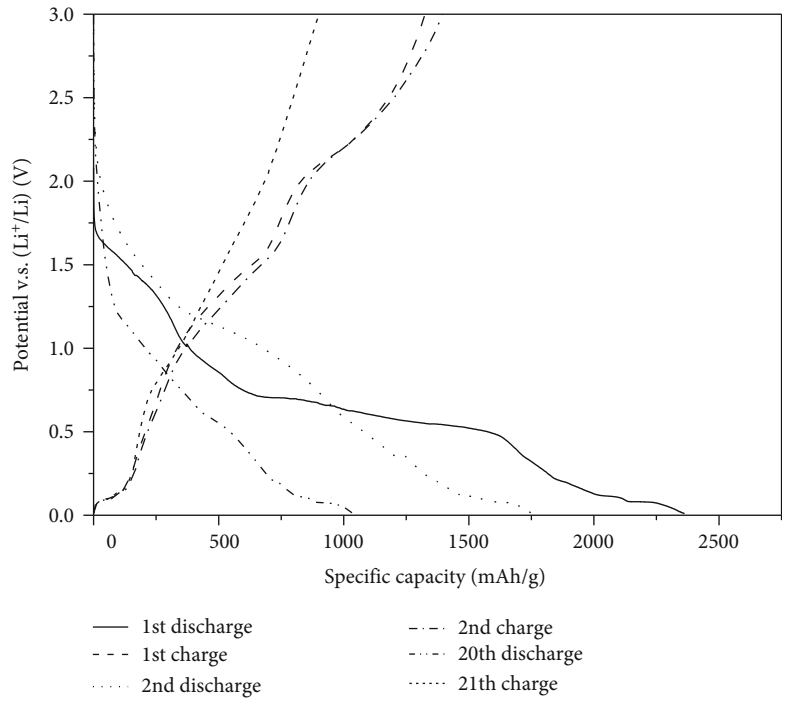

(b)

Figure 5: Continued.

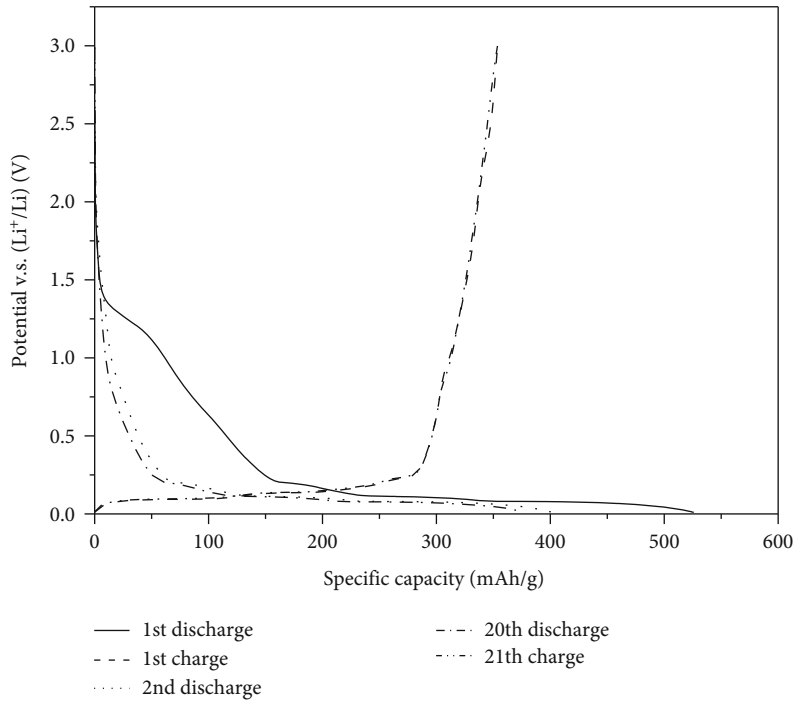

(c)

Figure 5: The discharge/charge profiles (between 0.01 V and 3 V at 0.1 C) with different charge-discharge cycles of the coin cell for (a) graphene, (b) N-doped graphene, and (c) Al_2O_3/graphene.

using an electrochemical analyzer (CH Instruments CHI 608B, USA) with the in situ XRD coil cell at 0.5 C.

3. Results and Discussion

Graphene grown on nickel foil by CVD and then graphene modified by nitrogen-doping as well as alumina deposited onto graphene by sputtering are shown in Figure 1. The presence of the G peak and the 2D peak (see Figure 2(a)) indicates the typical Raman characteristics for graphene (see the FESEM image of graphene in Figure 3(a)) [12]. Compared with Figure 2(a), Figure 2(b) shows the additional peak (D), which is attributed to defects of N-doped graphene (confirmed by the FESEM image of N-doped graphene in Figure 3(b) in comparison to the FESEM image of graphene in Figure 3(a)) and is in good agreement with the previous literature [13]. Compared with N-doped graphene, graphene exhibits no noticeable D peak at 1350 cm^{-1} (see Figures 2(a) and 2(b)) due to fewer defects, which is similar to the previous literature [13]. Furthermore, Figure 4(a) shows N-5 and N-6 XPS spectra of N-doped graphene, which demonstrates that the N species in the N-doped graphene are N-5 (13.7 area %) and N-6 (86.3 area %) [11]. Figure 4(b) shows the Al 2p XPS spectrum of Al_2O_3/graphene, which demonstrates the existence of Al_2O_3 in the composites (confirmed by the FESEM image of Al_2O_3/graphene in Figure 3(c) in comparison to the FESEM image of graphene in Figure 3(a)) and is in good agreement with the previous literature [14]. The FESEM image of graphene (see Figure 3(a)) grown at 900°C is similar to the previous literature [3]. Compared with the FESEM image of graphene, the FESEM image of N-doped graphene shows more defects (see Figures 3(a) and 3(b)). Compared with the FESEM image of graphene, the FESEM image of Al_2O_3/graphene shows an Al_2O_3 coating layer, which is similar to the previous literature [2].

Figures 5(a), 5(b), and 5(c) show the discharge/charge profiles (0.1 C) of the coin cell for graphene, N-doped graphene, and Al_2O_3/graphene. The appearance of the plateaus in the predischarge curves can be assigned to forming the SEI film on the surface of electrodes and the degrading electrolyte [15]. The predischarge plateaus rapidly disappear in the following cycles (See Figures 5(a), 5(b), and 5(c)) which also are verified by the cathode peaks (1.1 V for graphene, 0.6 V for N-doped graphene, and 1.2 V for Al_2O_3/graphene) happening during the 1st (predischarge) cycle and disappearing in the subsequent cycles (see Figures 6(a), 6(b), and 6(c)). The cathode peak (1.2 V) in the 1st (predischarge) cycle of Al_2O_3/graphene is not sharper than the other cathode peaks (1.1 V for graphene and 0.6 V for N-doped graphene) in the 1st (predischarge) cycles (see Figures 6(a), 6(b), and 6(c)) since Al_2O_3 coating layer could act as a preformed SEI to block the electrolyte and then suppress undesired side reactions with the electrolyte and thus reduce SEI formation during predischarging. So the potential plateau in the predischarge curve of Al_2O_3/graphene is not more obvious than

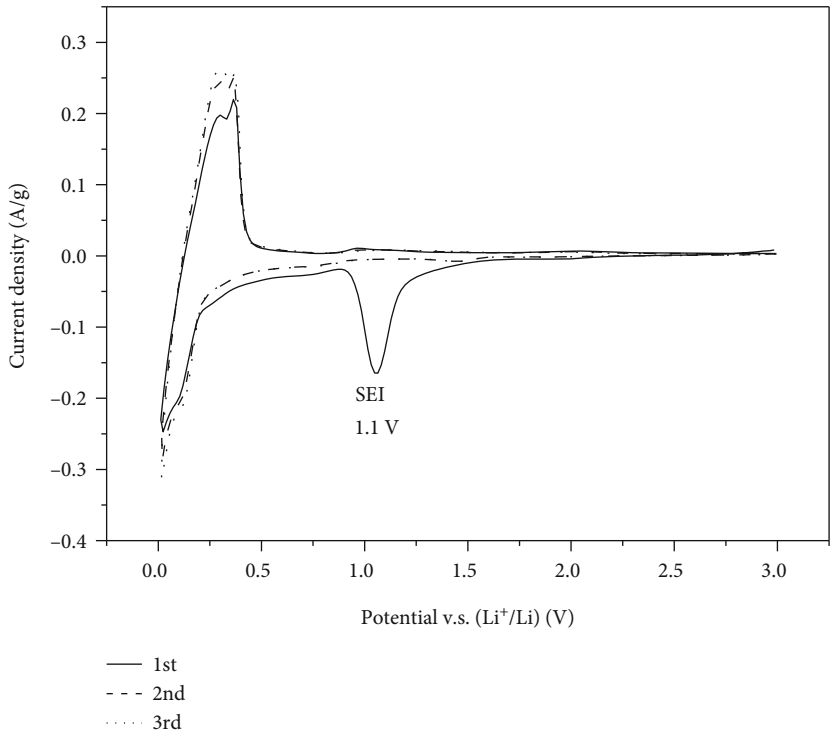

(a)

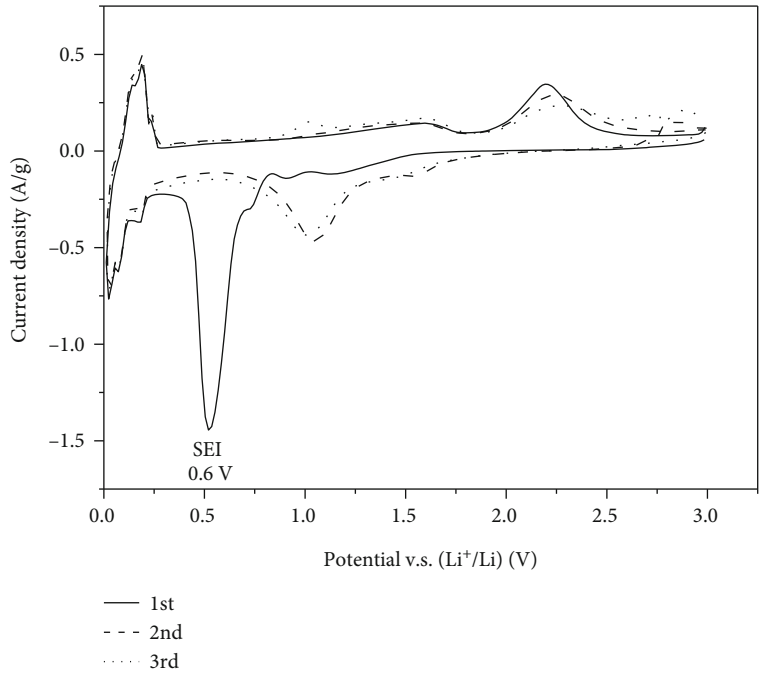

(b)

Figure 6: Continued.

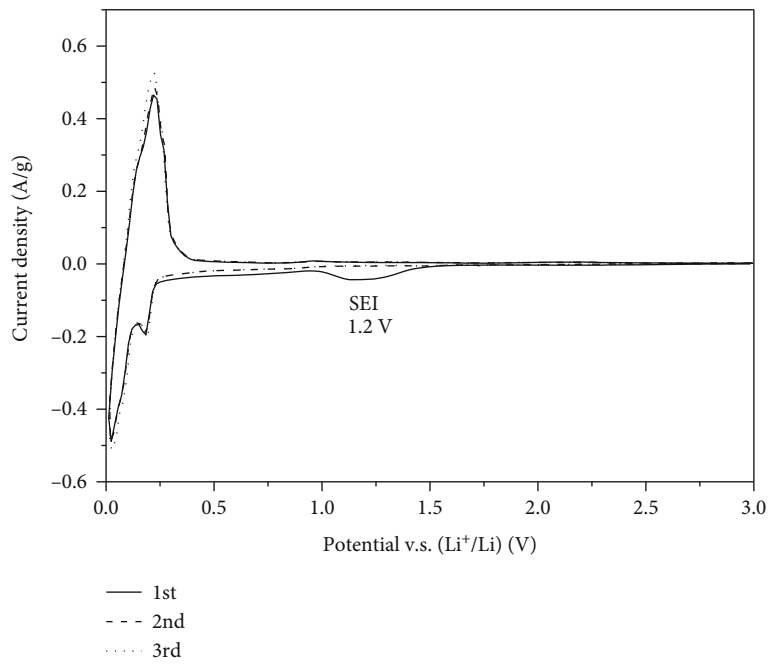

(c)

Figure 6: Cyclic voltammograms (between 0.01 V and 3 V from the 1st cycle to the 3rd cycle) of the coin cell for (a) graphene, (b) N-doped graphene, and (c) Al_2O_3/graphene.

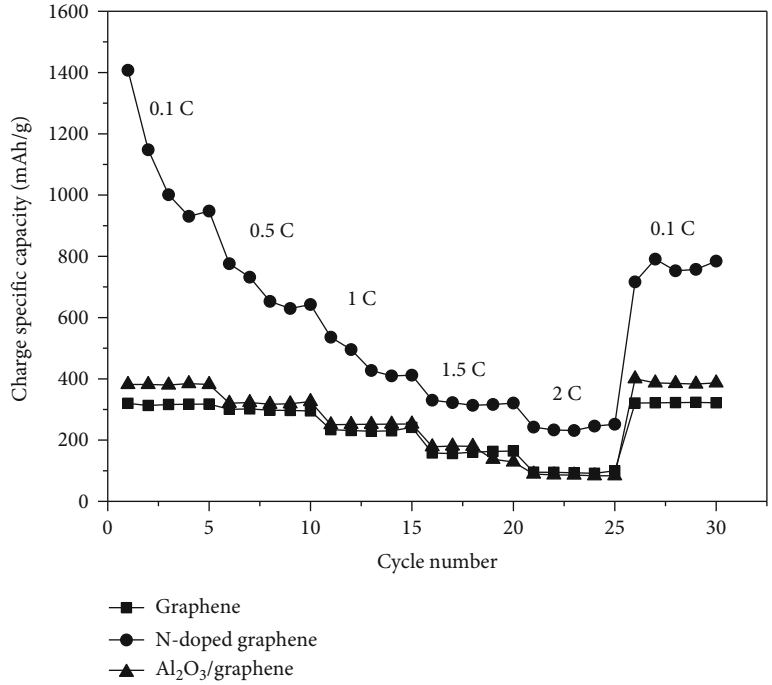

Figure 7: Rate capability (between 0.01 V and 3 V) with different charge-discharge cycles of the coin cell for graphene, N-doped graphene, and Al_2O_3/graphene.

those of graphene and N-doped graphene (see Figures 5(a), 5(b), and 5(c)). The cathode peak (0.6 V) in the 1st (predischarge) cycle of N-doped graphene is sharper than the cathode peak (1.1 V) in the 1st (predischarge) cycle of graphene (see Figures 6(a) and 6(b)) because compared with graphene, N-doped graphene possesses the additional peak (D) (see Figures 2(a) and 2(b)) which is attributed to defects then increasing SEI formation during predischarging.

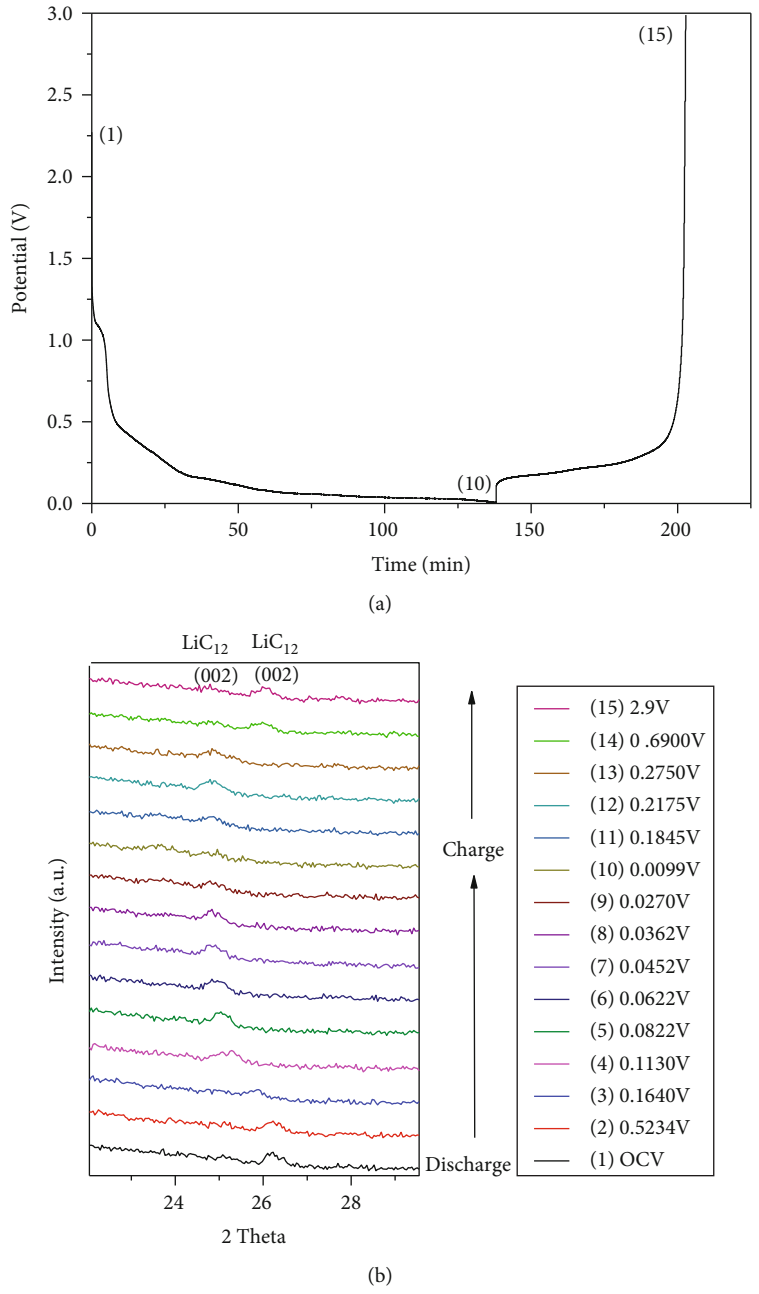

Figure 8: (a) Chronopotentiometry graph and (b) in situ XRD pattern of graphene.

The average charge-specific capacity of 6th to 10th cycles at 0.5 C is about 298 $mAhg^{-1}$ for graphene (see Figure 7); however, the average charge specific capacity of 6th to 10th cycles at 0.5 C is about 687 $mAhg^{-1}$ for N-doped graphene (see Figure 7). The reason behind this behavior may be explained as follows. 2 Theta of in situ XRD characteristic peaks for graphene moved toward a lower angle only about 25 (see Figure 8), but 2 Theta of in situ XRD characteristic peaks for N-doped graphene moved toward a lower angle about 24 (see Figure 9). Since gaps between graphene layers (d) are inversely proportional to 2 Theta of in situ XRD characteristic peaks according to Bragg's Law, then d for N-doped graphene is larger than d for graphene, and thus, the average charge-specific capacity (687 $mAhg^{-1}$) for N-doped graphene is larger than that (298 $mAhg^{-1}$) for graphene, which is similar to the previous literature [6]. It also could be explained by this: compared with graphene, N-doped graphene shows the additional in situ XRD characteristic peak (LiC_6) which possesses higher Li storage capacity in comparison to the characteristic peak (LiC_{12}) [16] (see Figures 8 and 9). Furthermore, for Al_2O_3/graphene, the average charge-specific capacity of 6th to 10th cycles at 0.5 C is about 321 $mAhg^{-1}$ which is also

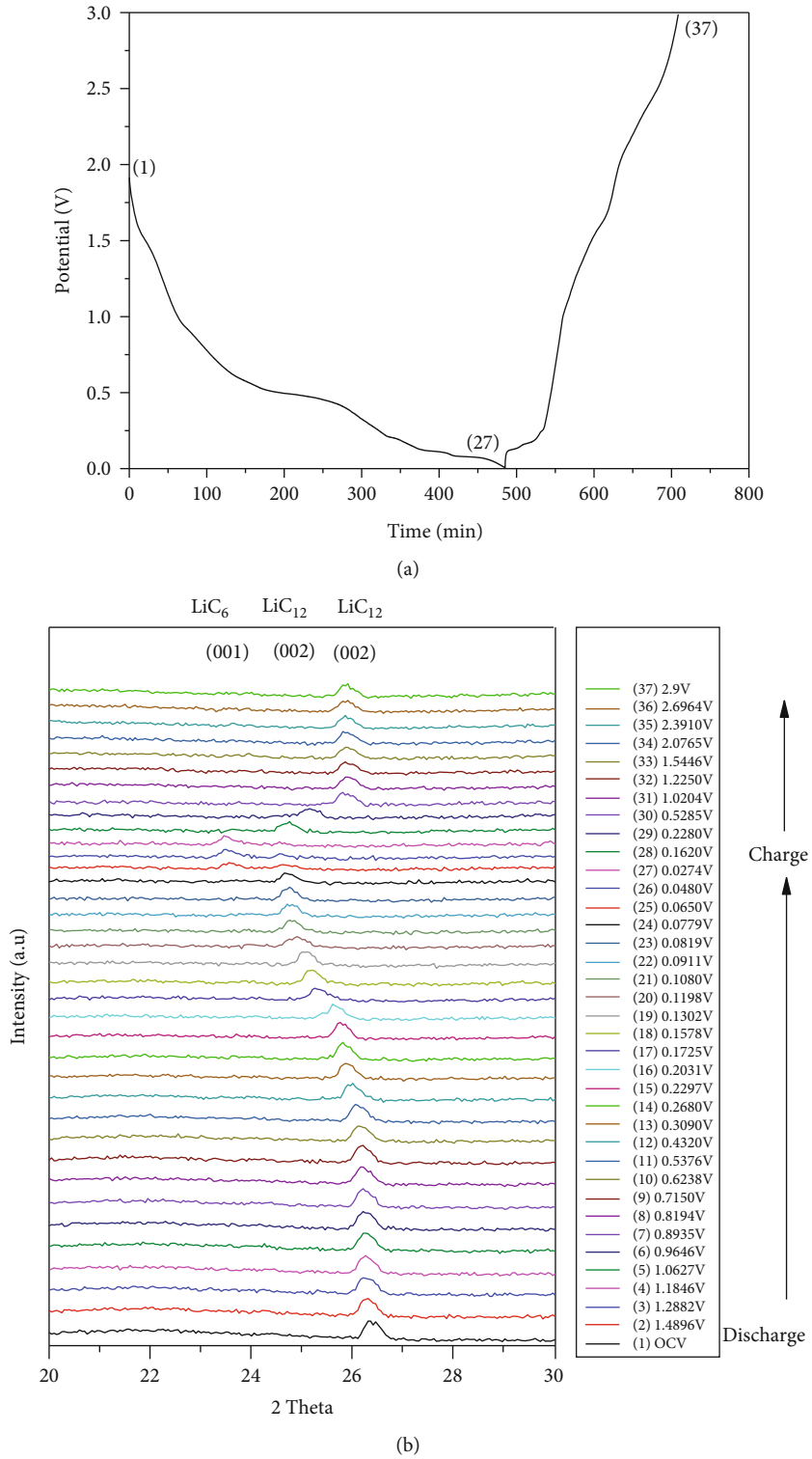

Figure 9: (a) Chronopotentiometry graph and (b) in situ XRD pattern of N-doped graphene.

larger than that (298 $mAhg^{-1}$) for graphene (see Figure 6). The reason behind this behavior may be that 2 Theta of in situ XRD characteristic peaks for Al_2O_3/graphene moved toward a lower angle (about 24) (see Figure 10) which is also small than that (about 25) for graphene (see Figure 8), and Al_2O_3/graphene also demonstrates the additional in situ XRD characteristic peak (LiC_6) which has higher Li storage capacity compared with characteristic peak (LiC_{12}) (see Figures 8 and 10). A similar result has been published in previous literature [10].

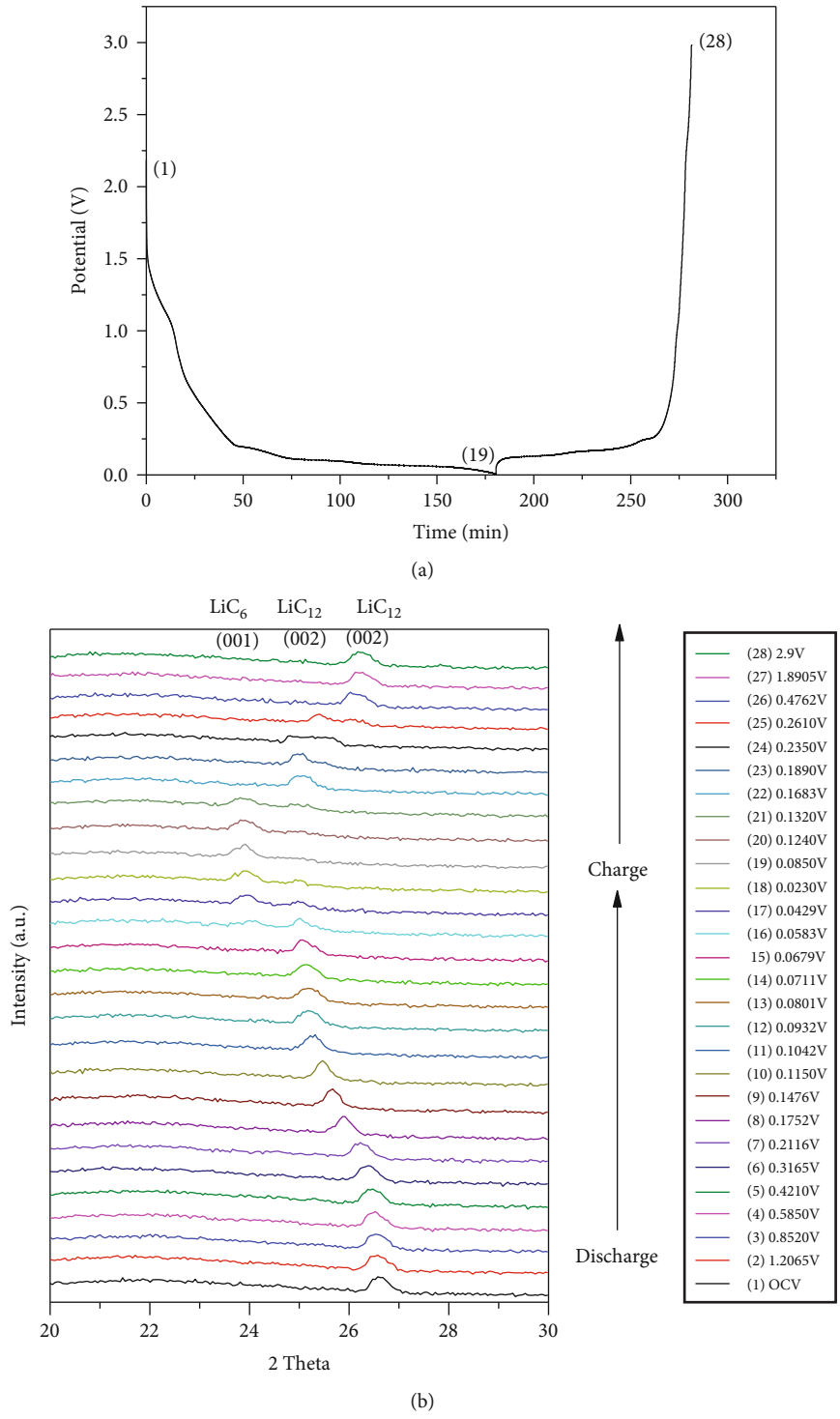

Figure 10: (a) Chronopotentiometry graph and (b) in situ XRD pattern of Al_2O_3/graphene.

4. Conclusions

The presence of the G peak and the 2D peak indicates the typical Raman characteristics for graphene. The N-5 and N-6 XPS spectra of N-doped graphene demonstrate that the N species in the N-doped graphene are N-5 and N-6. The Al 2p XPS spectrum of Al_2O_3/graphene shows the existence of Al_2O_3 in the composites. Furthermore, since Al_2O_3 coating layer could act as a preformed SEI to suppress undesired side reactions with the electrolyte and then reduce SEI formation during predischarging, the cathode peak in the predischarge cycle of Al_2O_3/graphene is not sharper than the other cathode peaks of graphene as well as N-doped graphene, and thus, the potential plateau in the predischarge curve of Al_2O_3/graphene is not more obvious than those of graphene as well as N-doped graphene.

Data Availability

Underlying data in detail are available when they are required.

Conflicts of Interest

The authors declare that they have no conflicts of interest.

Acknowledgments

Financial support by the Ministry of Science and Technology of the People's Republic of China (under grant no. MOST 110 - 2918 - I -224 - 001) is gratefully acknowledged.

References

[1] D. Miranda, C. M. Costa, and S. Lanceros-Mendez, "Lithium ion rechargeable batteries: state of the art and future needs of microscopic theoretical models and simulations," *Journal of Electroanalytical Chemistry*, vol. 739, pp. 97–110, 2015.

[2] C. C. Lin, S. P. Hsu, and G. J. Chen, "Effects of Alumina Films on N-Doped Carbon nanotubes/graphene composites as anode materials of Lithium-Ion batteries," *Journal of Nanomaterials*, vol. 2020, Article ID 6690401, 13 pages, 2020.

[3] C. C. Lin and P. L. Chang, "Synthesis of carbon nanotube/graphene composites on Ni foam without additional catalysts by CVD and their nitrogen-plasma treatment for anode materials in lithium-ion batteries," *Electrochemistry*, vol. 86, no. 3, pp. 109–115, 2018.

[4] J. R. Dahn, "Phase diagram ofLixC6," *Physical Review B*, vol. 44, no. 17, pp. 9170–9177, 1991.

[5] F. Wu, M. Liu, Y. Li et al., "High-mass-loading electrodes for advanced secondary batteries and supercapacitors," *Electrochemical Energy Reviews*, vol. 4, no. 2, pp. 382–446, 2021.

[6] H. Xu, L. Ma, and Z. Jin, "Nitrogen-doped graphene: synthesis, characterizations and energy applications," *Journal of Energy Chemistry*, vol. 27, no. 1, pp. 146–160, 2018.

[7] Y. J. Cho, H. S. Kim, H. Im et al., "Nitrogen-doped graphitic layers deposited on silicon nanowires for efficient lithium-ion battery anodes," *The Journal of Physical Chemistry C*, vol. 115, no. 19, pp. 9451–9457, 2011.

[8] N. Su, Y. Lyu, R. Gu, and B. Guo, "Al2O3 coated Li1.2Ni0.2Mn0.2Ru0.4O2 as cathode material for Li-ion batteries," *Journal of Alloys and Compounds*, vol. 741, pp. 398–403, 2018.

[9] A. M. Wise, C. Ban, J. N. Weker et al., "Effect of Al2O3Coating on Stabilizing LiNi0.4Mn0.4Co0.2O2Cathodes," *Chemistry of Materials*, vol. 27, no. 17, pp. 6146–6154, 2015.

[10] I. Lahiri, S. M. Oh, J. Y. Hwang et al., "Ultrathin alumina-coated carbon nanotubes as an anode for high capacity Li-ion batteries," *Journal of Materials Chemistry*, vol. 21, no. 35, p. 13621, 2011, article 13621.

[11] Z. S. Wu, W. Ren, L. Xu, F. Li, and H. M. Cheng, "Doped graphene sheets as anode materials with superhigh rate and large capacity for lithium ion batteries," *ACS Nano*, vol. 5, no. 7, pp. 5463–5471, 2011.

[12] W. Wang, S. Guo, M. Penchev et al., "Three dimensional few layer graphene and carbon nanotube foam architectures for high fidelity supercapacitors," *Nano Energy*, vol. 2, no. 2, pp. 294–303, 2013.

[13] K. Share, A. P. Cohn, R. Carter, B. Rogers, and C. L. Pint, "Role of nitrogen-doped graphene for improved high-capacity potassium ion battery anodes," *ACS Nano*, vol. 10, no. 10, pp. 9738–9744, 2016.

[14] K. Djebaili, Z. Mekhalif, A. Boumaza, and A. X. P. S. Djelloul, "XPS, FTIR, EDX, and XRD analysis of Al2O3 scales grown on PM2000 alloy," *Journal of spectroscopy*, vol. 2015, Article ID 868109, 16 pages, 2015.

[15] X. M. Liu, Z. D. Huang, S. W. Oh et al., "Carbon nanotube (CNT)-based composites as electrode material for rechargeable Li-ion batteries: a review," *Composites Science and Technology*, vol. 72, no. 2, pp. 121–144, 2012.

[16] J. Park, S. S. Park, and Y. S. Won, "In situ XRD study of the structural changes of graphite anodes mixed with SiOx during lithium insertion and extraction in lithium ion batteries," *Electrochimica Acta*, vol. 107, pp. 467–472, 2013.